Table 1: Vertical excitation energies and dominant contributions of the S_0 and S_1 states of fulvene optimized with SA2-CASSCF(6,6)/6-31G* and MRCI(CAS(6,6))/6-31G*. For MRCI, the Pople correction is also given (MRCI/+Pople).

State	ΔE (eV)	Configuration	%
		SA2-CASSCF(6,6) – S_0 optimization	
S_0	0.000	$(19a)^2(20a)^2(21a)^2(22a)^0(23a)^0(24a)^0$	77.3
S_1	4.110	$(19a)^2(20a)^2(21a)^1(22a)^1(23a)^0(24a)^0$	74.0
		$(19a)^2(20a)^1(21a)^1(22a)^2(23a)^0(24a)^0$	14.1
		SA2-CASSCF(6,6) – S_1 optimization	
S_0	1.446	$(19a)^2(20a)^2(21a)^2(22a)^0(23a)^0(24a)^0$	66.5
		$(19a)^2(20a)^1(21a)^2(22a)^1(23a)^0(24a)^0$	13.8
S_1	2.611	$(19a)^2(20a)^2(21a)^1(22a)^1(23a)^0(24a)^0$	72.3
		$(19a)^2(20a)^1(21a)^1(22a)^2(23a)^0(24a)^0$	15.8
		SA2-CASSCF(6,6) – MXS optimization - Planar	
S_0	2.880	$(19a)^2(20a)^2(21a)^1(22a)^1(23a)^0(24a)^0$	73.0
		$(19a)^2(20a)^1(21a)^1(22a)^2(23a)^0(24a)^0$	15.4
S_1	2.880	$(19a)^2(20a)^2(21a)^2(22a)^0(23a)^0(24a)^0$	60.1
		$(19a)^2(20a)^1(21a)^2(22a)^1(23a)^0(24a)^0$	16.8
		SA2-CASSCF(6,6) – MXS optimization – nonplanar (fixed 20°)	
S_0	2.796	$(19a)^2(20a)^2(21a)^2(22a)^0(23a)^0(24a)^0$	59.8
		$(19a)^2(20a)^1(21a)^2(22a)^1(23a)^0(24a)^0$	17.2
S_1	2.796	$(19a)^2(20a)^2(21a)^1(22a)^1(23a)^0(24a)^0$	72.9
		$(19a)^2(20a)^1(21a)^1(22a)^2(23a)^0(24a)^0$	15.4
		SA2-CASSCF(6,6) – MXS optimization – nonplanar (fixed 45°)	
S_0	2.549	$(19a)^2(20a)^2(21a)^2(22a)^0(23a)^0(24a)^0$	51.1
		$(19a)^2(20a)^1(21a)^2(22a)^1(23a)^0(24a)^0$	17.4
S_1	2.549	$(19a)^2(20a)^2(21a)^1(22a)^1(23a)^0(24a)^0$	64.7
		$(19a)^2(20a)^1(21a)^1(22a)^2(23a)^0(24a)^0$	13.6
		SA2-CASSCF(6,6) – MXS optimization – nonplanar (63°)	
S_0	2.445	$(19a)^2(20a)^2(21a)^1(22a)^1(23a)^0(24a)^0$	73.4
		$(19a)^2(20a)^1(21a)^1(22a)^2(23a)^0(24a)^0$	13.5
S_1	2.456	$(19a)^2(20a)^2(21a)^2(22a)^0(23a)^0(24a)^0$	48.1
		$(19a)^2(20a)^1(21a)^2(22a)^1(23a)^0(24a)^0$	28.3
		SA2-CASSCF(6,6) – MXS optimization – nonplanar (fixed 70°)	
S_0	2.470	$(19a)^2(20a)^2(21a)^1(22a)^1(23a)^0(24a)^0$	79.7
S_1	2.470	$(19a)^2(20a)^1(21a)^2(22a)^1(23a)^0(24a)^0$	47.0
		$(19a)^2(20a)^2(21a)^2(22a)^0(23a)^0(24a)^0$	28.3

SA2-CASSCF(6,6) – MXS optimization – nonplanar (fixed 90°)			
S_0	2.553	$(19a)^2(20a)^2(21a)^1(22a)^1(23a)^0(24a)^0$	87.8
S_1	2.553	$(19a)^2(20a)^2(21a)^1(22a)^1(23a)^0(24a)^0$	85.5
MRCI – S_0 optimization			
S_0	0.000/0.000	$(19a)^2(20a)^2(21a)^2(22a)^0(23a)^0(24a)^0$	69.1
S_1	3.841/3.633	$(19a)^2(20a)^2(21a)^1(22a)^1(23a)^0(24a)^0$	71.1
MRCI – S_1 optimization			
S_0	1.235/1.152	$(19a)^2(20a)^2(21a)^2(22a)^0(23a)^0(24a)^0$	62.3
S_1	2.609/2.459	$(19a)^2(20a)^2(21a)^1(22a)^1(23a)^0(24a)^0$	67.8
		$(19a)^2(20a)^1(21a)^1(22a)^2(23a)^0(24a)^0$	10.1
MRCI – MXS optimization - Planar			
S_0	3.022/2.972	$(19a)^2(20a)^2(21a)^1(22a)^1(23a)^0(24a)^0$	62.8
S_1	3.022/2.860	$(19a)^2(20a)^2(21a)^2(22a)^0(23a)^0(24a)^0$	52.8
		$(19a)^2(20a)^1(21a)^2(22a)^1(23a)^0(24a)^0$	11.9
MRCI – MXS optimization – Nonplanar (fixed 20°)			
S_0	2.930/2.891	$(19a)^2(20a)^2(21a)^1(22a)^1(23a)^0(24a)^0$	65.9
		$(19a)^2(20a)^1(21a)^1(22a)^2(23a)^0(24a)^0$	10.4
S_1	2.930/2.769	$(19a)^2(20a)^2(21a)^2(22a)^0(23a)^0(24a)^0$	55.4
		$(19a)^2(20a)^1(21a)^2(22a)^1(23a)^0(24a)^0$	12.8
MRCI – MXS optimization – Nonplanar (fixed 45°)			
S_0	2.649/2.584	$(19a)^2(20a)^2(21a)^1(22a)^1(23a)^0(24a)^0$	40.4
		$(19a)^2(20a)^2(21a)^2(22a)^0(23a)^0(24a)^0$	21.3
S_1	2.649/2.559	$(19a)^2(20a)^2(21a)^2(22a)^0(23a)^0(24a)^0$	33.0
		$(19a)^2(20a)^2(21a)^1(22a)^1(23a)^0(24a)^0$	26.1
MRCI – MXS optimization – nonplanar (65.1°)			
S_0	2.519/2.521	$(19a)^2(20a)^2(21a)^1(22a)^1(23a)^0(24a)^0$	66.9
S_1	2.519/2.423	$(19a)^2(20a)^2(21a)^2(22a)^0(23a)^0(24a)^0$	45.1
		$(19a)^2(20a)^1(21a)^2(22a)^1(23a)^0(24a)^0$	23.7
MRCI – MXS optimization – Nonplanar (fixed 70°)			
S_0	2.527/2.446	$(19a)^2(20a)^2(21a)^2(22a)^0(23a)^0(24a)^0$	39.3
		$(19a)^2(20a)^1(21a)^2(22a)^1(23a)^0(24a)^0$	29.2
S_1	2.527/2.534	$(19a)^2(20a)^2(21a)^1(22a)^1(23a)^0(24a)^0$	67.7
MRCI – MXS optimization – Nonplanar (fixed 90°)			
S_0	2.618/2.628	$(19a)^2(20a)^2(21a)^1(22a)^1(23a)^0(24a)^0$	63.2
		$(19a)^2(20a)^1(21a)^2(22a)^1(23a)^0(24a)^0$	13.0
S_1	2.618/2.595	$(19a)^2(20a)^1(21a)^2(22a)^1(23a)^0(24a)^0$	62.9
		$(19a)^2(20a)^2(21a)^1(22a)^1(23a)^0(24a)^0$	13.1

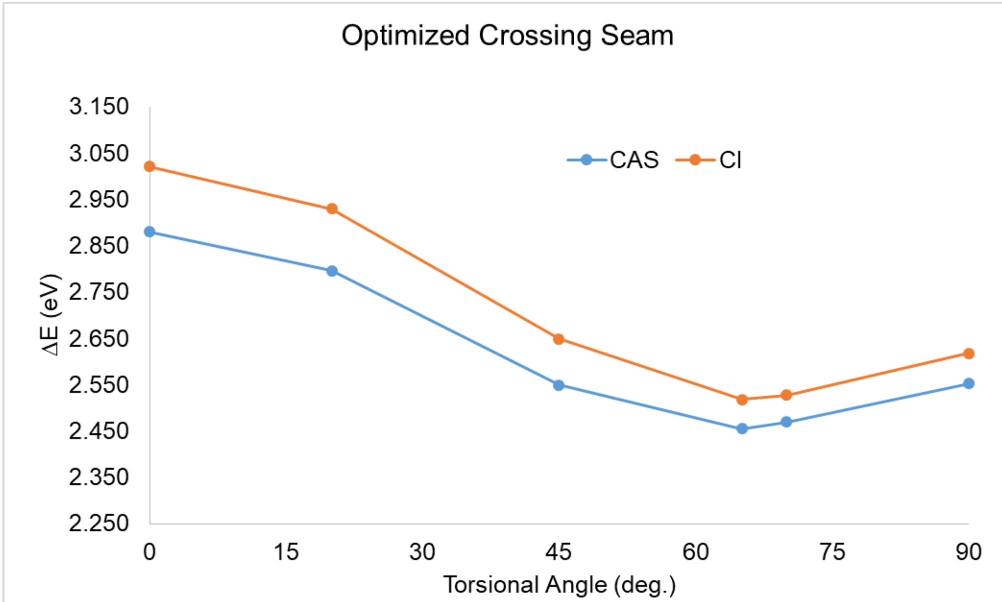

Figure 1: Relative energy of the optimized crossing seam between the S_0 and S_1 states using the SA2-CASSCF(6,6)/6-31G* and MRCI(CAS(6,6))/6-31G* methods. Energies relative to the optimized S_0 ground state in each method.

Table 2: Total energies in Hartree of fulvene

	S_0	S_1
SA2-CASSCF(6,6)-S_0 opt	-230.72231	-230.57127
SA2-CASSCF(6,6)-S_1 opt	-230.66916	-230.62635
SA2-CASSCF(6,6)-MXS-planar	-230.61647	-230.61647
SA2-CASSCF(6,6)-MXS-nonplanar (20°)	-230.61957	-230.61955
SA2-CASSCF(6,6)-MXS-nonplanar (45°)	-230.62862	-230.62862
SA2-CASSCF(6,6)-MXS-nonplanar (63°)	-230.63208	-230.63206
SA2-CASSCF(6,6)-MXS-nonplanar (70°)	-230.63154	-230.63154
SA2-CASSCF(6,6)-MXS-nonplanar (90°)	-230.62850	-230.62850
MRCI-S_0 opt	-231.33320	-231.19206
MRCI+Q-S_0 opt	-231.46471	-231.33121
MRCI-S_1 opt	-231.28780	-231.23732
MRCI+Q-S_1 opt	-231.42239	-231.37102
MRCI-MXS-planar	-231.22216	-231.22216
MRCI+Q-MXS-planar	-231.35550	-231.35960
MRCI-MXS-nonplanar (20°)	-231.22553	-231.22553
MRCI+Q-MXS-nonplanar (20°)	-231.35848	-231.36297
MRCI-MXS-nonplanar (45°)	-231.23585	-231.23585
MRCI+Q-MXS-nonplanar (45°)	-231.36976	-231.37068
MRCI-MXS-nonplanar (65.1°)	-231.24064	-231.24064
MRCI+Q-MXS-nonplanar (65.1°)	-231.37206	-231.37566
MRCI-MXS-nonplanar (70°)	-231.24033	-231.24033
MRCI+Q-MXS-nonplanar (70°)	-231.37480	-231.37157
MRCI-MXS-nonplanar (90°)	-231.23698	-231.23698
MRCI+Q-MXS-nonplanar (90°)	-231.36814	-231.36934

Table 3: Oscillator strength of the S_0 to S_1 transition of fulvene optimized with SA2-CASSCF(6,6)/6-31G* and MRCI(CAS(6,6))/6-31G*.

Method	*f*
SA2-CASSCF(6,6) – S_0 optimization	0.00
SA2-CASSCF(6,6) – S_1 optimization	0.00
MRCI – S_0 optimization	0.01
MRCI – S_1 optimization	0.00

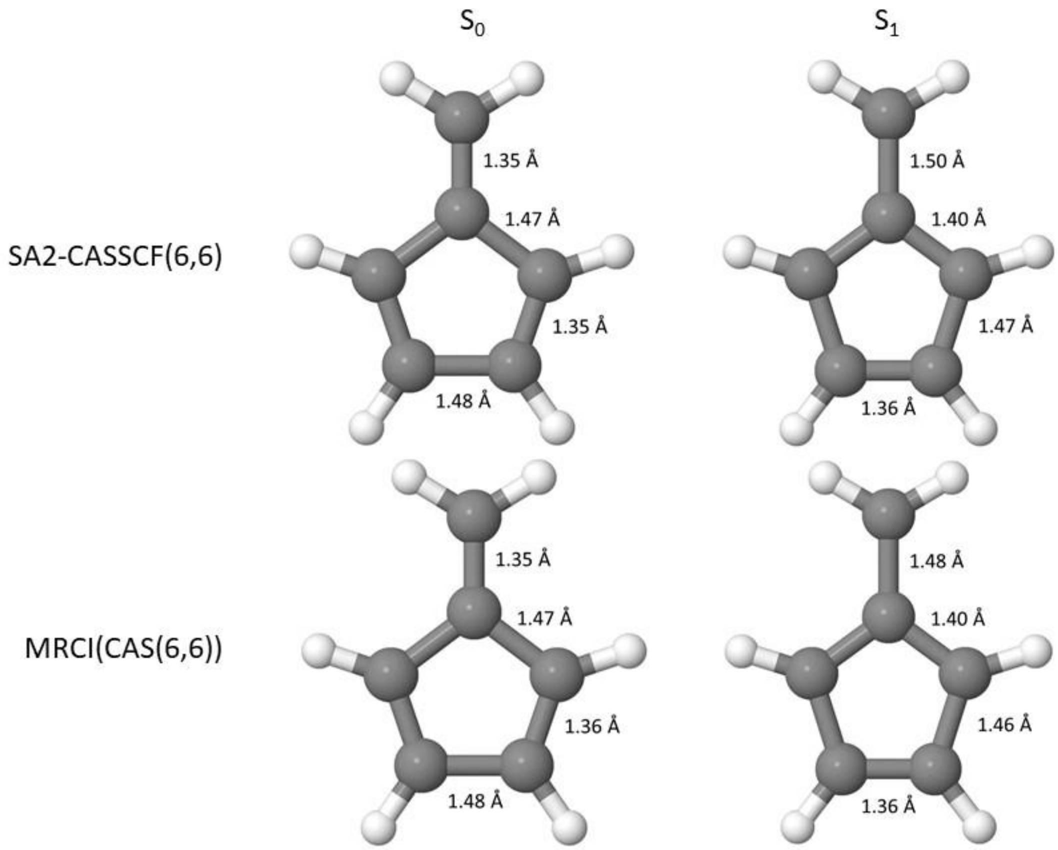

Figure 2: Bond distances of the S_0 to S_1 states optimized with SA2-CASSCF(6,6)/6-31G* and MRCI(CAS(6,6))/6-31G*.

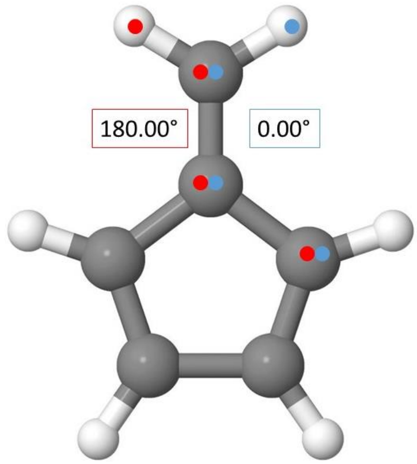

Figure 3: Torsional angles of the S_0 to S_1 states optimized with SA2-CASSCF(6,6)/6-31G* and MRCI(CAS(6,6))/6-31G*. The molecule is planar, so there is no variation. Torsional angles, blue and red, are designated with colored dots.

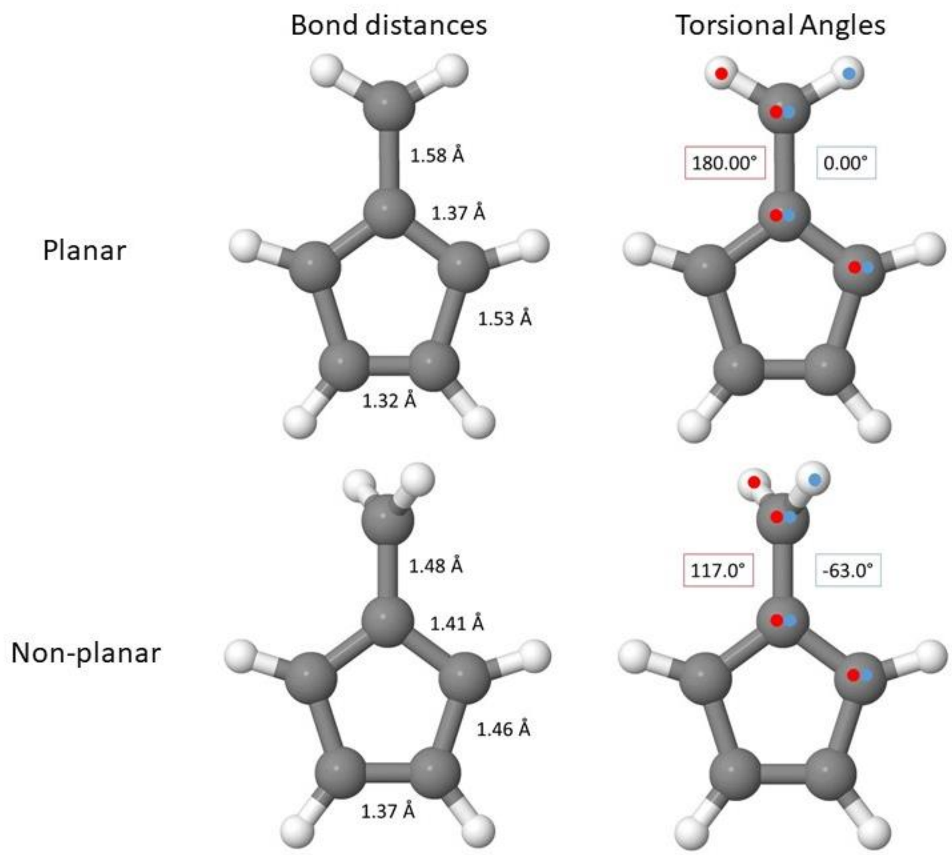

Figure 4: Bond distances and torsional angles of the optimized crossing seam between the S_0 to S_1 states optimized with SA2-CASSCF(6,6)/6-31G*. Torsional angles, blue and red, are designated with colored dots.

Table 4: C-C bond distances for each fixed torsional angle about the CH2 group using the SA2-CASSCF(6,6)/6-31G* and MRCI(CAS(6,6))/6-31G* methods.

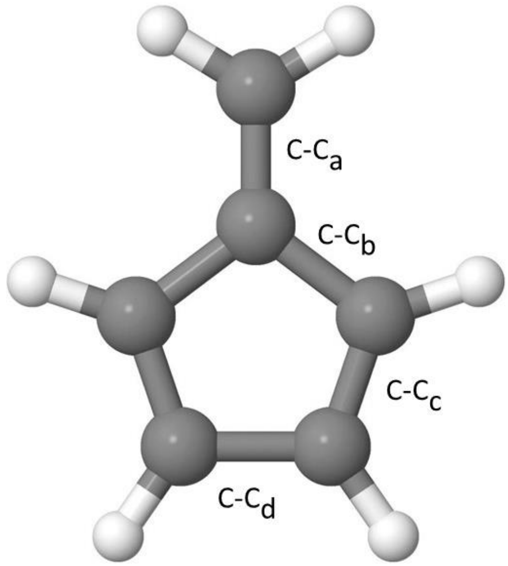

Torsional Angle	C-C_a	C-C_b	C-C_c	C-C_d
		SA2-CASSCF(6,6)		
20.0°	1.56	1.37	1.52	1.32
45.0°	1.51	1.39	1.49	1.34
63.0°	1.48	1.41	1.46	1.37
70.0°	1.47	1.41	1.44	1.38
90.0°	1.48	1.42	1.42	1.41
		MRCI		
20.0°	1.56	1.37	1.53	1.32
45.0°	1.51	1.38	1.50	1.33
65.1°	1.47	1.40	1.46	1.37
70.0°	1.47	1.41	1.45	1.38
90.0°	1.47	1.42	1.42	1.41

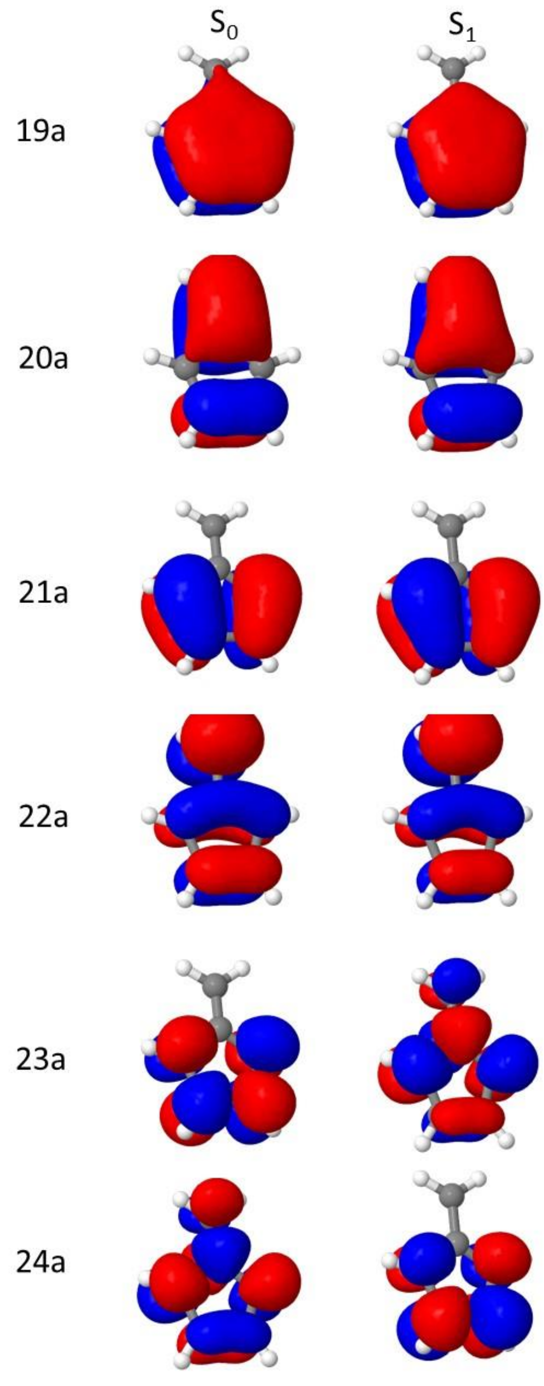

Figure 5: Optimized active orbitals for the S_0 and S_1 states, respectively, optimized with SA2-CASSCF(6,6)/6-31G*.

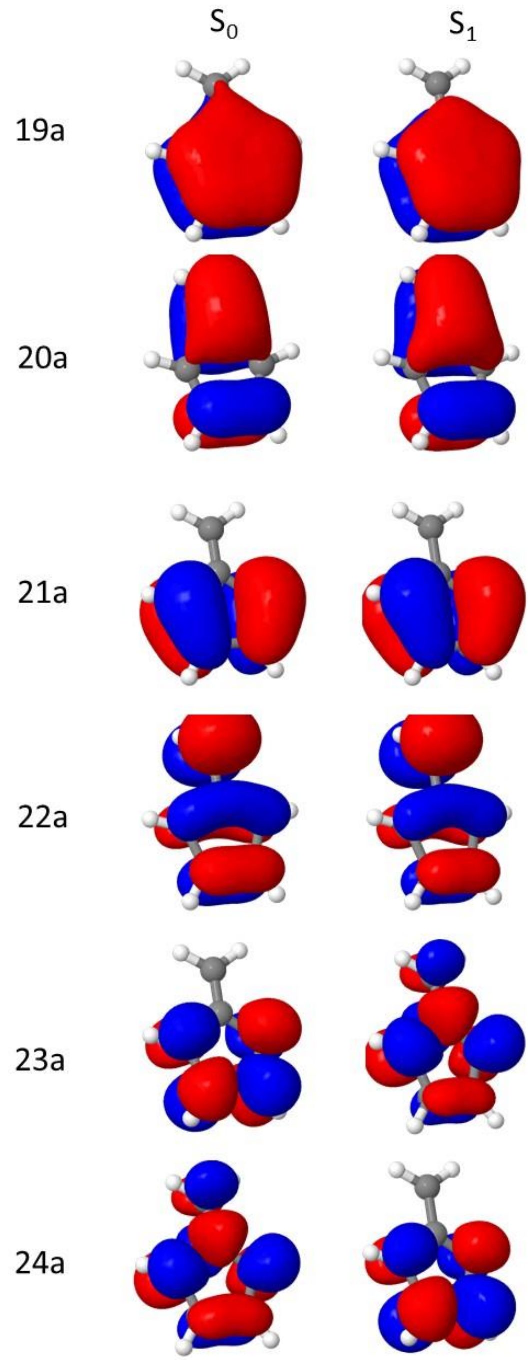

Figure 6: Optimized active orbitals for the S_0 and S_1 states, respectively, optimized with MRCI(CAS(6,6))/6-31G*.

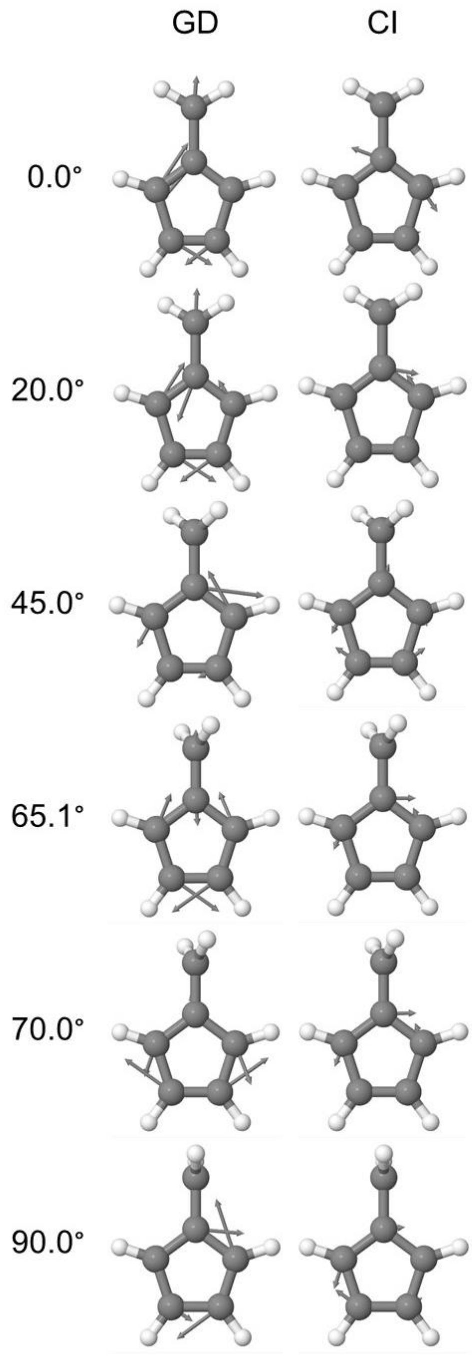

Figure 7: Plots of the GD and CI vectors of fulvene at the optimized crossing seam for several torsional angles going to the $-CH_2$ group. The MRCI(CAS(6,6))/6-31G* was utilized. The lowest energy structure at the crossing seam corresponds to 65.1°.